eJSE
International

Blast Loading and Blast Effects on Structures – An Overview

T. Ngo, P. Mendis, A. Gupta & J. Ramsay
The University of Melbourne, Australia

ABSTRACT: The use of vehicle bombs to attack city centers has been a feature of campaigns by terrorist organizations around the world. A bomb explosion within or immediately nearby a building can cause catastrophic damage on the building's external and internal structural frames, collapsing of walls, blowing out of large expanses of windows, and shutting down of critical life-safety systems. Loss of life and injuries to occupants can result from many causes, including direct blast-effects, structural collapse, debris impact, fire, and smoke. The indirect effects can combine to inhibit or prevent timely evacuation, thereby contributing to additional casualties. In addition, major catastrophes resulting from gas-chemical explosions result in large dynamic loads, greater than the original design loads, of many structures. Due to the threat from such extreme loading conditions, efforts have been made during the past three decades to develop methods of structural analysis and design to resist blast loads. The analysis and design of structures subjected to blast loads require a detailed understanding of blast phenomena and the dynamic response of various structural elements. This paper presents a comprehensive overview of the effects of explosion on structures. An explanation of the nature of explosions and the mechanism of blast waves in free air is given. This paper also introduces different methods to estimate blast loads and structural response.

1 EXPLOSIONS AND BLAST PHENOMENON

An explosion is defined as a large-scale, rapid and sudden release of energy. Explosions can be categorized on the basis of their nature as physical, nuclear or chemical events. In physical explosions, energy may be released from the catastrophic failure of a cylinder of compressed gas, volcanic eruptions or even mixing of two liquids at different temperatures. In a nuclear explosion, energy is released from the formation of different atomic nuclei by the redistribution of the protons and neutrons within the interacting nuclei, whereas the rapid oxidation of fuel elements (carbon and hydrogen atoms) is the main source of energy in the case of chemical explosions.

Explosive materials can be classified according to their physical state as solids, liquids or gases. Solid explosives are mainly high explosives for which blast effects are best known. They can also be classified on the basis of their sensitivity to ignition as secondary or primary explosive. The latter is one that can be easily detonated by simple ignition from a spark, flame or impact. Materials such as mercury fulminate and lead azide are primary explosives. Secondary explosives when detonated create blast (shock) waves which can result in widespread damage to the surroundings. Examples include trinitrotoluene (TNT) and ANFO.

The detonation of a condensed high explosive generates hot gases under pressure up to 300 kilo bar and a temperature of about 3000-4000C°. The hot gas expands forcing out the volume it occupies. As a consequence, a layer of compressed air (blast wave) forms in front of this gas volume containing most of the energy released by the explosion. Blast wave instantaneously increases to a value of pressure above the ambient atmospheric pressure. This is referred to as the side-on overpressure that decays as the shock wave expands outward from the explosion source. After a short time, the pressure behind the front may drop below the ambient pressure (Figure 1). During such a negative phase, a partial vacuum is created and air is sucked in. This is also accompanied by high suction winds that carry the debris for long distances away from the explosion source.
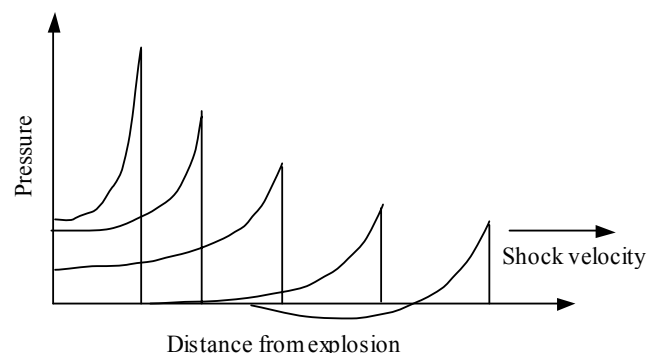
Figure 1: Blast wave propagation
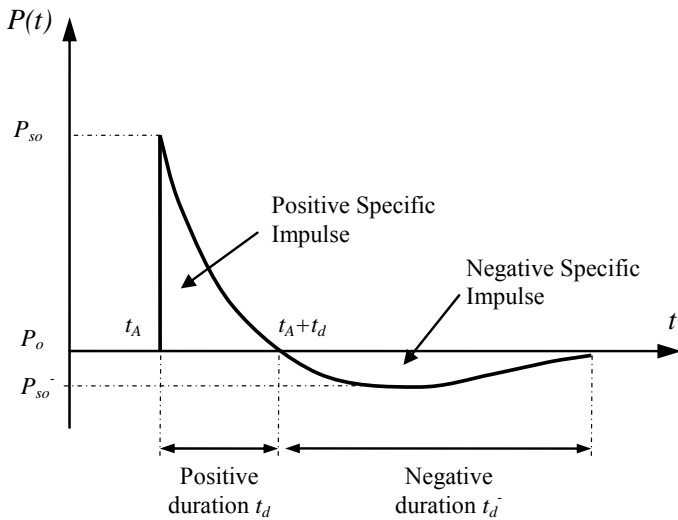
Figure 2: Blast wave pressure – Time history

2 EXPLOSIVE AIR BLAST LOADING

The threat for a conventional bomb is defined by two equally important elements, the bomb size, or charge weight *W,* and the standoff distance *R* between the blast source and the target (Figure 3). For example, the blast occurred at the basement of World Trade Centre in 1993 has the charge weight of 816.5 kg TNT. The Oklahoma bomb in 1995 has a charge weight of 1814 kg at a stand off of 4.5m (Longinow, 1996). As terrorist attacks may range from the small letter bomb to the gigantic truck bomb as experienced in Oklahoma City, the mechanics of a conventional explosion and their effects on a target must be addressed.

The observed characteristics of air blast waves are found to be affected by the physical properties of the explosion source. Figure 2 shows a typical blast pressure profile. At the arrival time t_A, following the explosion, pressure at that position suddenly increases to a peak value of overpressure, P_{so}, over the ambient pressure, P_o. The pressure then decays to ambient level at time t_d, then decays further to an under pressure P_{so}^- (creating a partial vacumn) before eventually returning to ambient conditions at time $t_d + t_d^-$. The quantity P_{so} is usually referred to as the peak side-on overpressure, incident peak overpressure or merely peak overpressure (TM 5-1300, 1990).

The incident peak over pressures P_{so} are amplified by a reflection factor as the shock wave encounters an object or structure in its path. Except for specific focusing of high intensity shock waves at near 45° incidence, these reflection factors are typically greatest for normal incidence (a surface adjacent and perpendicular to the source) and diminish with the angle of obliquity or angular position relative to the

source. Reflection factors depend on the intensity of the shock wave, and for large explosives at normal incidence these reflection factors may enhance the incident pressures by as much as an order of magnitude.

Throughout the pressure-time profile, two main phases can be observed; portion above ambient is called positive phase of duration t_d, while that below ambient is called negative phase of duration, t_d^-. The negative phase is of a longer duration and a lower intensity than the positive duration. As the stand-off distance increases, the duration of the positive-phase blast wave increases resulting in a lower-amplitude, longer-duration shock pulse . Charges situated extremely close to a target structure impose a highly impulsive, high intensity pressure load over a localized region of the structure; charges situated further away produce a lower-intensity, longer-duration uniform pressure distribution over the entire structure. Eventually, the entire structure is engulfed in the shock wave, with reflection and diffraction effects creating focusing and shadow zones in a complex pattern around the structure. During the negative phase, the weakened structure may be subjected to impact by debris that may cause additional damage.
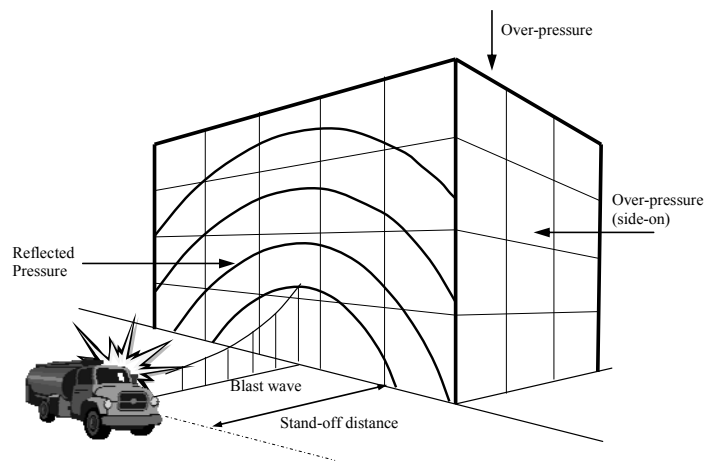
Figure 3: Blast loads on a building

If the exterior building walls are capable of resisting the blast load, the shock front penetrates through window and door openings, subjecting the floors, ceilings, walls, contents, and people to sudden pressures and fragments from shattered windows, doors, etc. Building components not capable of resisting the blast wave will fracture and be further fragmented and moved by the dynamic pressure that immediately follows the shock front. Building contents and people will be displaced and tumbled in the direction of blast wave propagation. In this manner the blast will propagate through the building.

2.1 Blast Wave Scaling Laws

All blast parameters are primarily dependent on the amount of energy released by a detonation in the form of a blast wave and the distance from the explosion. A universal normalized description of the blast effects can be given by scaling distance relative to $(E/P_0)^{1/3}$ and scaling pressure relative to P_0, where E is the energy release (kJ) and P_0 the ambient pressure (typically 100 kN/m²). For convenience, however, it is general practice to express the basic explosive input or charge weight W as an equivalent mass of TNT. Results are then given as a function of the dimensional distance parameter (scaled distance) $Z = R/W^{1/3}$, where R is the actual effective distance from the explosion. W is generally expressed in kilograms. Scaling laws provide parametric correlations between a particular explosion and a standard charge of the same substance.

2.2 Prediction of Blast Pressure

Blast wave parameters for conventional high explosive materials have been the focus of a number of studies during the 1950's and 1960's. Estimations of peak overpressure due to spherical blast based on scaled distance $Z = R/W^{1/3}$ were introduced by Brode (1955) as:

$$P_{so} = \frac{6.7}{Z^3} + 1 \text{ bar } (P_{so} > 10 \text{ bar})$$

$$P_{so} = \frac{0.975}{Z} + \frac{1.455}{Z^2} + \frac{5.85}{Z^3} - 0.019 \text{ bar} \qquad (1)$$

$$(0.1 \text{ bar} < P_{so} < 10 \text{ bar})$$

Newmark and Hansen (1961) introduced a relationship to calculate the maximum blast overpressure, P_{so}, in bars, for a high explosive charge detonates at the ground surface as:

$$P_{so} = 6784 \frac{W}{R^3} + 93\left(\frac{W}{R^3}\right)^{\frac{1}{2}} \qquad (2)$$

Another expression of the peak overpressure in kPa is introduced by Mills (1987), in which W is expressed as the equivalent charge weight in kilograms of TNT, and Z is the scaled distance:

$$P_{so} = \frac{1772}{Z^3} - \frac{114}{Z^2} + \frac{108}{Z} \qquad (3)$$

As the blast wave propagates through the atmosphere, the air behind the shock front is moving outward at lower velocity. The velocity of the air particles, and hence the wind pressure, depends on the peak overpressure of the blast wave. This later velocity of the air is associated with the dynamic pressure, $q(t)$. The maximum value, q_s, say, is given by

$$q_s = 5p_{so}^2 / 2(p_{so} + 7p_o) \qquad (4)$$

If the blast wave encounters an obstacle perpendicular to the direction of propagation, reflection increases the overpressure to a maximum reflected pressure P_r as:

$$P_r = 2P_{so}\left\{\frac{7P_o + 4P_{so}}{7P_o + P_{so}}\right\} \qquad (5)$$

A full discussion and extensive charts for predicting blast pressures and blast durations are given by Mays and Smith (1995) and TM5-1300 (1990). Some representative numerical values of peak reflected overpressure are given in Table 1.

Table 1. Peak reflected overpressures P_r (in MPa) with different W-R combinations

W / R	100 kg TNT	500 kg TNT	1000 kg TNT	2000 kg TNT
1m	165.8	354.5	464.5	602.9
2.5m	34.2	89.4	130.8	188.4
5m	6.65	24.8	39.5	60.19
10m	0.85	4.25	8.15	14.7
15m	0.27	1.25	2.53	5.01
20m	0.14	0.54	1.06	2.13
25m	0.09	0.29	0.55	1.08
30m	0.06	0.19	0.33	0.63

For design purposes, reflected overpressure can be idealized by an equivalent triangular pulse of maximum peak pressure P_r and time duration t_d, which yields the reflected impulse i_r

$$i_r = \frac{1}{2}P_r t_d \qquad (6)$$

Duration t_d is related directly to the time taken for the overpressure to be dissipated. Overpressure arising from wave reflection dissipates as the perturbation propagates to the edges of the obstacle at a velocity related to the speed of sound (U_s) in the compressed and heated air behind the wave front. Denoting the maximum distance from an edge as S (for example, the lesser of the height or half the width of a conventional building), the additional pressure due to reflection is considered to reduce from $P_r - P_{so}$ to zero in time $3S/U_s$. Conservatively, U_s can be taken as the normal speed of sound, which is about 340 m/s, and the additional impulse to the structure evaluated on the assumption of a linear decay.

After the blast wave has passed the rear corner of a prismatic obstacle, the pressure similarly propagates on to the rear face; linear build-up over duration $5S/U_s$ has been suggested. For skeletal structures the effective duration of the net overpressure load is thus small, and the drag loading

based on the dynamic pressure is then likely to be dominant. Conventional wind-loading pressure co-efficients may be used, with the conservative assumption of instantaneous build-up when the wave passes the plane of the relevant face of the building, the loads on the front and rear faces being numerically cumulative for the overall load effect on the structure. Various formulations have been put forward for the rate of decay of the dynamic pressure loading; a parabolic decay (i.e. corresponding to a linear decay of equivalent wind velocity) over a time equal to the total duration of positive overpressure is a practical approximation.

3 GAS EXPLOSION LOADING AND EFFECT OF INTERNAL EXPLOSIONS

In the circumstances of progressive build-up of fuel in a low-turbulence environment, typical of domestic gas explosions, flame propagation on ignition is slow and the resulting pressure pulse is correspondingly extended. The specific energy of combustion of a hydrocarbon fuel is very high (46000 kJ/kg for propane, compared to 4520 kJ/kg for TNT) but widely differing effects are possible according to the conditions at ignition.

Internal explosions likely produce complex pressure loading profiles as a result of the resulting two loading phases. The first results from the blast over-pressure reflection and, due to the confinement provided by the structure, re-reflection will occur. Depending on the degree of confinement of the structure, the confined effects of the resulting pressures may cause different degrees of damage to the structure. On the basis of the confinement effect, target structures can be described as either vented or un-vented. The latter must be stronger to resist a specific explosion yield than a vented structure where some of the explosion energy would be dissipated by breaking of window glass or fragile partitions.

Venting following the failure of windows (at typically 7 kN/m^2) generally greatly reduces the peak values of internal pressures. Study of this problem at the Building Research Establishment (Ellis and Crowhurst, 1991) showed that an explosion fuelled by a 200 ml aerosol canister in a typical domestic room produced a peak pressure of 9 kN/m^2 with a pulse duration over 0.1s. This is long by comparison with the natural frequency of wall panels in conventional building construction and a quasi-static design pressure is commonly advocated. Much higher pressures with a shorter timescale are generated in turbulent conditions. Suitable conditions arise in buildings in multi-room explo-

sions on passage of the blast through doorways, but can also be created by obstacles closer to the release of the gas. They may be presumed to occur on release of gas by failure of industrial pressure vessels or pipelines.

4 STRUCTURAL RESPONSE TO BLAST LOADING

Complexity in analyzing the dynamic response of blast-loaded structures involves the effect of high strain rates, the non-linear inelastic material behavior, the uncertainties of blast load calculations and the time-dependent deformations. Therefore, to simplify the analysis, a number of assumptions related to the response of structures and the loads has been proposed and widely accepted. To establish the principles of this analysis, the structure is idealized as a single degree of freedom (SDOF) system and the link between the positive duration of the blast load and the natural period of vibration of the structure is established. This leads to blast load idealization and simplifies the classification of the blast loading regimes.

4.1 *Elastic SDOF Systems*

The simplest discretization of transient problems is by means of the SDOF approach. The actual structure can be replaced by an equivalent system of one concentrated mass and one weightless spring representing the resistance of the structure against deformation. Such an idealized system is illustrated in Figure 4. The structural mass, M, is under the effect of an external force, $F(t)$, and the structural resistance, R, is expressed in terms of the vertical displacement, y, and the spring constant, K.

The blast load can also be idealized as a triangular pulse having a peak force F_m and positive phase duration t_d (see Figure 4). The forcing function is given as

$$F(t) = F_m \left(1 - \frac{t}{t_d}\right) \qquad (7)$$

The blast impulse is approximated as the area under the force-time curve, and is given by

$$I = \frac{1}{2} F_m t_d \qquad (8)$$

The equation of motion of the un-damped elastic SDOF system for a time ranging from 0 to the positive phase duration, t_d, is given by Biggs (1964) as

$$M\ddot{y} + Ky = F_m \left(1 - \frac{t}{t_d}\right) \qquad (9)$$

The general solution can be expressed as:

Displacement

$$y(t) = \frac{F_m}{K}(1 - \cos \omega t) + \frac{F_m}{Kt_d}\left(\frac{\sin \omega t}{\omega} - t\right)$$ (10)

Velocity

$$\dot{y}(t) = \frac{dy}{dt} = \frac{F_m}{K}\left[\omega \sin \omega t + \frac{1}{t_d}(\cos \omega t - 1)\right]$$

in which ω is the natural circular frequency of vibration of the structure and T is the natural period of vibration of the structure which is given by equation 11.

$$\omega = \frac{2\pi}{T} = \sqrt{\frac{K}{M}}$$ (11)
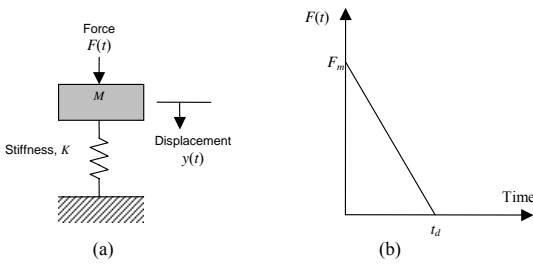
Figure 4: (a) SDOF system and (b) blast loading

The maximum response is defined by the maximum dynamic deflection y_m which occurs at time t_m. The maximum dynamic deflection y_m can be evaluated by setting dy/dt in Equation 10 equal to zero, i.e. when the structural velocity is zero. The dynamic load factor, DLF, is defined as the ratio of the maximum dynamic deflection y_m to the static deflection y_{st} which would have resulted from the static application of the peak load F_m, which is shown as follows:

$$DLF = \frac{y_{max}}{y_{st}} = \frac{y_{max}}{F_m/K} = \psi(\omega t_d) = \Psi\left(\frac{t_d}{T}\right)$$ (12)

The structural response to blast loading is significantly influenced by the ratio t_d/T or ωt_d ($t_d/T = \omega t_d / 2\pi$). Three loading regimes are categorized as follows:

- $\omega t_d < 0.4$: impulsive loading regime.
- $\omega t_d < 0.4$: quasi-static loading regime.
- $0.4 < \omega t_d < 40$: dynamic loading regime.

4.2 Elasto-Plastic SDOF Systems

Structural elements are expected to undergo large inelastic deformation under blast load or high velocity impact. Exact analysis of dynamic response is then only possible by step-by-step nu-

merical solution requiring a nonlinear dynamic finite-element software. However, the degree of uncertainty in both the determination of the loading and the interpretation of acceptability of the resulting deformation is such that solution of a postulated equivalent ideal elasto-plastic SDOF system (Biggs, 1964) is commonly used. Interpretation is based on the required ductility factor $\mu = y_m/y_e$ (Figure 5).
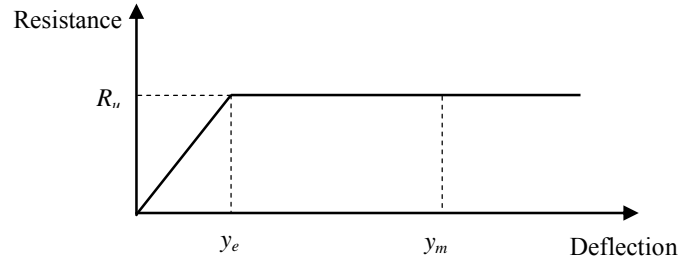
Figure 5: Simplified resistance function of an elasto-plastic SDOF system

For example, a uniform simply supported beam has first mode shape $\phi(x) = \sin \pi x/L$ and the equivalent mass $M = (1/2)mL$, where L is the span of the beam and m is mass per unit length. The equivalent force corresponding to a uniformly distributed load of intensity p is $F = (2/\pi)pL$. The response of the ideal bilinear elasto-plastic system can be evaluated in closed form for the triangular load pulse comprising rapid rise and linear decay, with maximum value F_m and duration t_d. The result for the maximum displacement is generally presented in chart form (TM 5-1300), as a family of curves for selected values of R_u/F_m showing the required ductility μ as a function of t_d/T, in which R_u is the structural resistance of the beam and T is the natural period (Figure 6).
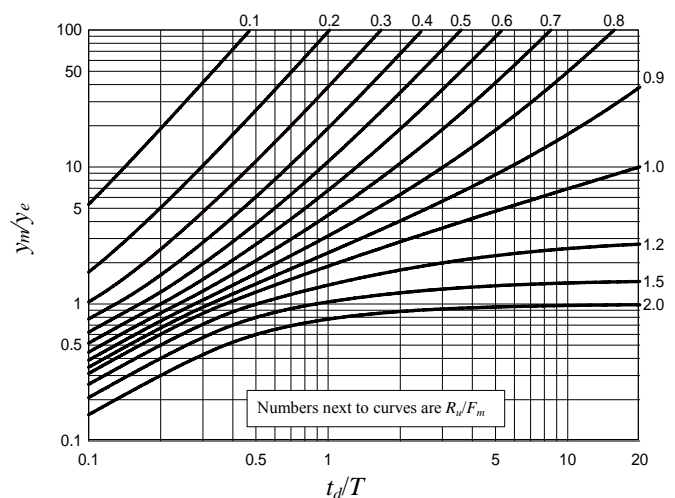
Figure 6: Maximum response of elasto-plastic SDF system to a triangular load.

5 MATERIAL BEHAVIORS AT HIGH STRAIN-RATE

Blast loads typically produce very high strain rates in the range of 10^2 - 10^4 s^{-1}. This high straining (loading) rate would alter the dynamic mechanical properties of target structures and, accordingly, the expected damage mechanisms for various structural elements. For reinforced concrete structures subjected to blast effects the strength of concrete and steel reinforcing bars can increase significantly due to strain rate effects. Figure 7 shows the approximate ranges of the expected strain rates for different loading conditions. It can be seen that ordinary static strain rate is located in the range : 10^{-6}-10^{-5} s^{-1}, while blast pressures normally yield loads associated with strain rates in the range : 10^2-10^4 s^{-1}.
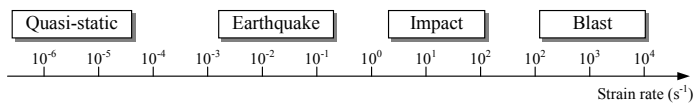
Figure 7: Strain rates associated with different types of loading

5.1 *Dynamic Properties of Concrete under High-Strain Rates*

The mechanical properties of concrete under dynamic loading conditions can be quite different from that under static loading. While the dynamic stiffness does not vary a great deal from the static stiffness, the stresses that are sustained for a certain period of time under dynamic conditions may gain values that are remarkably higher than the static compressive strength (Figure 8). Strength magnification factors as high as 4 in compression and up to 6 in tension for strain rates in the range : 10^2–10^3 /sec have been reported (Grote et al., 2001).
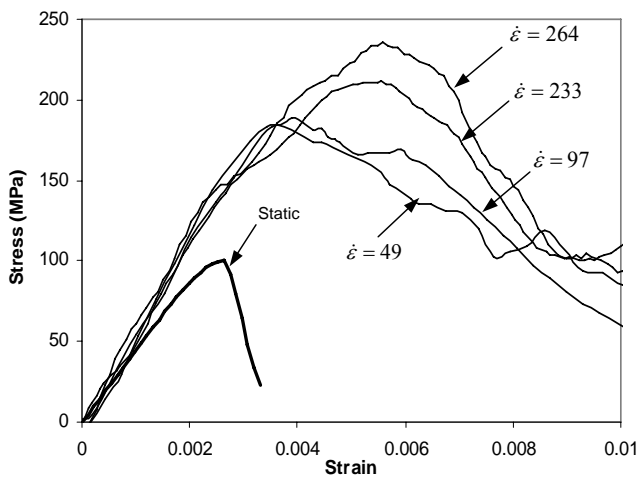
Figure 8: Stress-strain curves of concrete at different strain-rates (Ngo et al., 2004a)

For the increase in peak compressive stress (f'_c), a dynamic increase factor (DIF) is introduced in the

CEB-FIP (1990) model (Figure 9) for strain-rate enhancement of concrete as follows:

$$DIF = \left(\frac{\dot{\varepsilon}}{\dot{\varepsilon}_s}\right)^{1.026\alpha} \qquad \text{for } \dot{\varepsilon} \leq 30s^{-1} \qquad (13)$$

$$DIF = \gamma\left(\frac{\dot{\varepsilon}}{\dot{\varepsilon}_s}\right)^{1/3} \qquad \text{for } \dot{\varepsilon} > 30s^{-1} \qquad (14)$$

where:
$\dot{\varepsilon}$ = strain rate
$\dot{\varepsilon}_s$ = 30×10^{-6} s^{-1} (quasi-static strain rate)
$\log \gamma$ = 6.156 α - 2
α = $1/(5 + 9 f'_c/f_{co})$
f_{co} = 10 MPa = 1450 psi
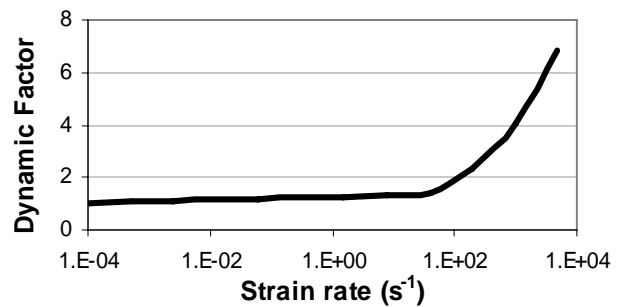
Figure 9: Dynamic Increase Factor for peak stress of concrete

5.2 *Dynamic Properties of Reinforcing Steel under High-Strain Rates*

Due to the isotropic properties of metallic materials, their elastic and inelastic response to dynamic loading can easily be monitored and assessed. Norris et al. (1959) tested steel with two different static yield strength of 330 and 278 MPa under tension at strain rates ranging from 10^{-5} to 0.1 s^{-1}. Strength increase of 9 - 21% and 10 - 23 % were observed for the two steel types, respectively. Dowling and Harding (1967) conducted tensile experiments using the tensile version of Split Hopkinton's Pressure Bar (SHPB) on mild steel using strain rates varying between 10^{-3} s^{-1} and 2000 s^{-1}. It was concluded from this test series that materials of body-centered cubic (BCC) structure (such as mild steel) showed the greatest strain rate sensitivity. It has been found that the lower yield strength of mild steel can almost be doubled; the ultimate tensile strength can be increased by about 50%; and the upper yield strength can be considerably higher. In contrast, the ultimate tensile strain decreases with increasing strain rate.

Malvar (1998) also studied strength enhancement of steel reinforcing bars under the effect of high strain rates. This was described in terms of the dynamic increase factor (DIF), which can be evaluated for different steel grades and for yield stresses, f_y, ranging from 290 to 710 MPa as represented by equation 15.

$$\text{DIF} = \left(\frac{\dot{\varepsilon}}{10^{-4}}\right)^{\alpha} \qquad (15)$$

where for calculating yield stress $\alpha = \alpha_{fy}$,
$$\alpha_{fy} = 0.074 - 0.04(f_y / 414) \qquad (16)$$

for ultimate stress calculation $\alpha = \alpha_{fu}$
$$\alpha_{fu} = 0.019 - 0.009(f_y / 414) \qquad (17)$$

6 FAILURE MODES OF BLAST-LOADED STRUCTURES

Blast loading effects on structural members may produce both local and global responses associated with different failure modes. The type of structural response depends mainly on the loading rate, the orientation of the target with respect to the direction of the blast wave propagation and boundary conditions. The general failure modes associated with blast loading can be flexure, direct shear or punching shear. Local responses are characterized by localized bleaching and spalling, and generally result from the close-in effects of explosions, while global responses are typically manifested as flexural failure.

6.1 Global Structural Behavior

The global response of structural elements is generally a consequence of transverse (out-of-plane) loads with long exposure time (quasi-static loading), and is usually associated with global membrane (bending) and shear responses. Therefore, the global response of above-ground reinforced concrete structures subjected to blast loading is referred to as membrane/bending failure.

The second global failure mode to be considered is shear failure. It has been found that under the effect of both static and dynamic loading, four types of shear failure can be identified: diagonal tension, diagonal compression, punching shear, and direct (dynamic) shear (Woodson, 1993). The first two types are common in reinforced concrete elements under static loading while punching shear is associated with local shear failure, the familiar example of this is column punching through a flat slab. These shear response mechanisms have relatively minor structural effect in case of blast loading and can be neglected. The fourth type of shear failure is direct (dynamic) shear. This failure mode is primarily associated with transient short duration dynamic loads that result from blast effects, and it depends mainly on the intensity of the pressure waves. The associ-

ated shear force is many times higher than the shear force associated with flexural failure modes. The high shear stresses may lead to direct global shear failure and it may occur very early (within a few milliseconds of shock wave arrival to the frontal surface of the structure) which can be prior to any occurrence of significant bending deformations.

6.2 Localized Structural Behavior

The close-in effect of explosion may cause localized shear or flexural failure in the closest structural elements. This depends mainly on the distance between the source of the explosion and the target, and the relative strength/ductility of the structural elements. The localized shear failure takes place in the form of localized punching and spalling, which produces low and high-speed fragments. The punching effect is frequently referred to as bleaching, which is well known in high velocity impact applications and the case of explosions close to the surface of structural members. Bleaching failures are typically accompanied by spalling and scabbing of concrete covers as well as fragments and debris (Figure 10).

Figure 10: Breaching failure due to a close-in explosion of 6000kg TNT equivalent

6.3 Pressure-Impulse (P-I) Diagrams

The pressure-impulse (*P-I*) diagram is an easy way to mathematically relate a specific damage level to a combination of blast pressures and impulses imposes on a particular structural element. An example of a P-I diagram is shown in Figure 11 to show levels of damage of a structural member. Region (I) corresponds to severe structural damage and region (II) refers to no or minor damage. There are other *P-I* diagrams that concern with human response to blast in which case there are three categories of blast-induced injury, namely : primary, secondary, and tertiary injury (Baker et al., 1983).
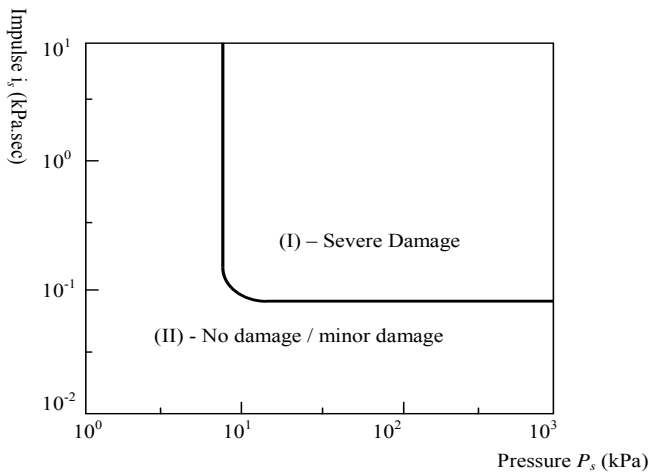
Figure 11: Typical pressure-impulse (*P-I*) diagram

7 BLAST WAVE-STRUCTURE INTERACTION

The structural behavior of an object or structure exposed to such blast wave may be analyzed by dealing with two main issues. Firstly, blast-loading effects, i.e., forces that are resulted directly from the action of the blast pressure; secondly, the structural response, or the expected damage criteria associated with such loading effects. It is important to consider the interaction of the blast waves with the target structures. This might be quite complicated in the case of complex structural configurations. However, it is possible to consider some equivalent simplified geometry. Accordingly, in analyzing the dynamic response to blast loading, two types of target structures can be considered: diffraction-type and drag-type structures. As these names imply, the former would be affected mainly by diffraction (engulfing) loading and the latter by drag loading. It should be emphasized that actual buildings will respond to both types of loading and the distinction is made primarily to simplify the analysis. The structural response will depend upon the size, shape and weight of the target, how firmly it is attached to the ground, and also on the existence of openings in each face of the structure.

Above ground or shallow-buried structures can be subjected to ground shock resulting from the detonation of explosive charges that are on/or close to ground surface. The energy imparted to the ground by the explosion is the main source of ground shock. A part of this energy is directly transmitted through the ground as directly-induced ground shock, while part is transmitted through the air as air-induced ground shock. Air-induced ground shock results when the air-blast wave compresses the ground surface and sends a stress pulse into the ground underlayers. Generally, motion due to air-induced ground is maximum at the ground surface and attenuates

with depth (TM 5-1300, 1990). The direct shock results from the direct transmission of explosive energy through the ground. For a point of interest on the ground surface, the net experienced ground shock results from a combination of both the air-induced and direct shocks.

7.1 Loads from Air-induced Ground Shock

To overcome complications of predicting actual ground motion, one-dimensional wave propagation theory has been employed to quantify the maximum displacement, velocity and acceleration in terms of the already known blast wave parameters (TM 5-1300). The maximum vertical velocity at the ground surface, V_v, is expressed in terms of the peak incident overpressure, P_{so}, as:

$$V_v = \frac{P_{so}}{\rho C_p} \tag{18}$$

where ρ and C_p are, respectively, the mass density and the wave seismic velocity in the soil.

By integrating the vertical velocity in Equation 18 with time, the maximum vertical displacement at the ground surface, D_v, can be obtained as:

$$D_v = \frac{i_s}{1000\rho C_p} \tag{19}$$

Accounting for the depth of soil layers, an empirical formula is given by (TM 5-1300) to estimate the vertical displacement in meters so that

$$D_v = 0.09 W^{\frac{1}{6}} (H/50)^{0.6} (P_{so})^{\frac{2}{3}} \tag{20}$$

where W is the explosion yield in 10^9 kg, and H is the depth of the soil layer in meters.

7.2 Loads from Direct Ground Shock

As a result of the direct transmission of the explosion energy, the ground surface experiences vertical and horizontal motions. Some empirical equations were derived (TM 5-1300) to predict the direct-induced ground motions in three different ground media; dry soil, saturated soil and rock media. The peak vertical displacement in m/s at the ground surface for rock, $D_{V_{rock}}$ and dry soil, $D_{V_{soil}}$ are given as

$$D_{V_{rock}} = \frac{0.25 R^{\frac{1}{3}} W^{\frac{1}{3}}}{Z^{\frac{1}{3}}} \tag{21}$$

$$D_{V_{soil}} = \frac{0.17 R^{\frac{1}{3}} W^{\frac{1}{3}}}{Z^{2.3}} \tag{22}$$

The maximum vertical acceleration, A_v, in m/s^2 for all ground media is given by

$$A_v = \frac{1000}{W^{\frac{1}{8}}Z^2} \qquad (23)$$

8 TECHNICAL DESIGN MANUALS FOR BLAST-RESISTANT DESIGN

This section summarizes applicable military design manuals and computational approaches to predicting blast loads and the responses of structural systems. Although the majority of these design guidelines were focused on military applications these knowledge are relevant for civil design practice.

Structures to Resist the Effects of Accidental Explosions, TM 5-1300 (U.S. Departments of the Army, Navy, and Air Force, 1990). This manual appears to be the most widely used publication by both military and civilian organizations for designing structures to prevent the propagation of explosion and to provide protection for personnel and valuable equipment. It includes step-by-step analysis and design procedures, including information on such items as (1) blast, fragment, and shock-loading; (2) principles of dynamic analysis; (3) reinforced and structural steel design; and (4) a number of special design considerations, including information on tolerances and fragility, as well as shock isolation. Guidance is provided for selection and design of security windows, doors, utility openings, and other components that must resist blast and forced-entry effects.

A Manual for the Prediction of Blast and Fragment Loadings on Structures, DOE/TIC-11268 (U.S. Department of Energy, 1992). This manual provides guidance to the designers of facilities subject to accidental explosions and aids in the assessment of the explosion-resistant capabilities of existing buildings.

Protective Construction Design Manual, ESL-TR-87-57 (Air Force Engineering and Services Center, 1989). This manual provides procedures for the analysis and design of protective structures exposed to the effects of conventional (non-nuclear) weapons and is intended for use by engineers with basic knowledge of weapons effects, structural dynamics, and hardened protective structures.

Fundamentals of Protective Design for Conventional Weapons, TM 5-855-1 (U.S. Department of the Army, 1986). This manual provides procedures for the design and analysis of protective structures subjected to the effects of conventional weapons. It is intended for use by engineers involved in designing hardened facilities.

The Design and Analysis of Hardened Structures to Conventional Weapons Effects (DAHS CWE, 1998). This new Joint Services manual, written by a team of more than 200 experts in conventional weapons and protective structures engineering, supersedes U.S. Department of the Army TM 5-855-1, Fundamentals of Protective Design for Conventional Weapons (1986), and Air Force Engineering and Services Centre ESL-TR-87-57, Protective Construction Design Manual (1989).

Structural Design for Physical Security—State of the Practice Report (ASCE, 1995). This report is intended to be a comprehensive guide for civilian designers and planners who wish to incorporate physical security considerations into their designs or building retrofit efforts.

9 COMPUTER PROGRAMS FOR BLAST AND SHOCK EFFECTS

Computational methods in the area of blast-effects mitigation are generally divided into those used for prediction of blast loads on the structure and those for calculation of structural response to the loads. Computational programs for blast prediction and structural response use both first-principle and semi-empirical methods. Programs using the first-principle method can be categorized into uncouple and couple analyses. The uncouple analysis calculates blast loads as if the structure (and its components) were rigid and then applying these loads to a responding model of the structure. The shortcoming of this procedure is that when the blast field is obtained with a rigid model of the structure, the loads on the structure are often over-predicted, particularly if significant motion or failure of the structure occurs during the loading period.

For a coupled analysis, the blast simulation module is linked with the structural response module. In this type of analysis the CFD (computational fluid mechanics) model for blast-load prediction is solved simultaneously with the CSM (computational solid mechanics) model for structural response. By accounting for the motion of the structure while the blast calculation proceeds, the pressures that arise due to motion and failure of the structure can be predicted more accurately. Examples of this type of computer codes are AUTODYN, DYNA3D, LS-DYNA and ABAQUS. Table 2 summarizes a listing of computer programs that are currently being used to model blast-effects on structures.

Table 2. Examples of computer programs used to simulate blast effects and structural response

Name	Purpose and type of analysis	Author/Vendor
BLASTX	Blast prediction, CFD code	SAIC
CTH	Blast prediction, CFD code	Sandia National Laboratories
FEFLO	Blast prediction, CFD code	SAIC
FOIL	Blast prediction, CFD code	Applied Research Associates, Waterways Experiment Station
SHARC	Blast prediction, CFD code	Applied Research Associates, Inc.
DYNA3D	Structural response + CFD (Couple analysis)	Lawrence Livermore National Laboratory (LLNL)
ALE3D	Coupled analysis	Lawrence Livermore National Laboratory (LLNL)
LS-DYNA	Structural response + CFD (Couple analysis)	Livermore Software Technology Corporation (LSTC)
Air3D	Blast prediction, CFD code	Royal Military of Science College, Cranfield University
CONWEP	Blast prediction (empirical)	US Army Waterways Experiment Station
AUTO-DYN	Structural response + CFD (Couple analysis)	Century Dynamics
ABAQUS	Structural response + CFD (Couple analysis)	ABAQUS Inc.

Prediction of the blast-induced pressure field on a structure and its response involves highly nonlinear behavior. Computational methods for blast-response prediction must therefore be validated by comparing calculations to experiments. Considerable skill is required to evaluate the output of the computer code, both as to its correctness and its appropriateness to the situation modeled; without such judgment, it is possible through a combination of modeling errors and poor interpretation to obtain erroneous or meaningless results. Therefore, successful computational modeling of specific blast scenarios by engineers unfamiliar with these programs is difficult, if not impossible.

10 CASE STUDY – RC COLUMN SUBJECTED TO BLAST LOADING

A ground floor column (6.4m high) of a multi-storey building (modified from a typical building designed in Australia) was analysed in this case study (see Fig. 12).

The parameters considered were the concrete strength (40MPa for NSC column and 80 MPa for HSC column) and spacing of ligatures (400mm for ordinary detailing-OMRF and 100mm for special seismic detailing-SMRF). It has been found that with increasing concrete compressive strength, the column size can be effectively reduced. In this case the column size was reduced from 500 x 900 mm for the NSC column down to 350 x 750 for the HSC column (Table 2) while the axial load capacities of the two columns are still the same.

The blast load was calculated based on data from the Oklahoma bombing report (ASCE 1996) with a stand off distance of 11.2m. The simplified triangle shape of the blast load profile was used (see Fig. 13). The duration of the positive phase of the blast is 1.3 milliseconds.

The 3D model of the column (see Fig. 14) was analysed using the nonlinear explicit code LS-Dyna 3D (2002) which takes into account both material nonlinearity and geometric nonlinearity. The strain-rate-dependent constitutive model proposed in the previous section was adopted. The effects of the blast loading were modelled in the dynamic analysis to obtain the deflection time history of the column.

Table 3. Concrete grades and member sizes

Column	Sizes	f'_c (MPa)	Ligature Spacing
NSC	500x900	40	400mm and 100mm
HSC	350x750	80	400mm and 100mm
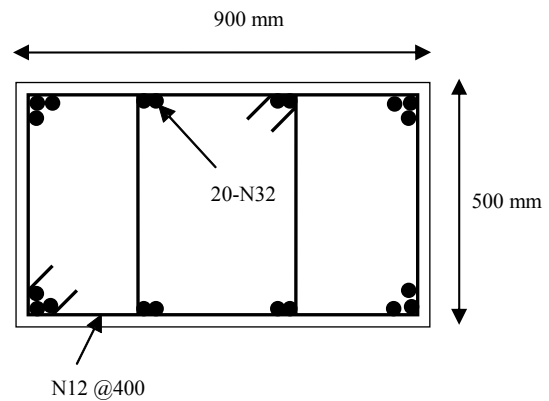
Figure 12. Cross section of the NSC column – Ordinary detailing (400 mm ligature spacing).
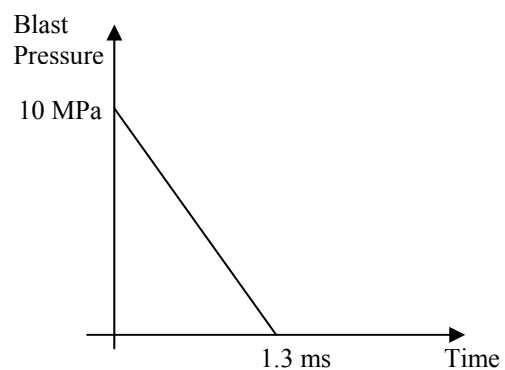
Figure 13. Blast loading
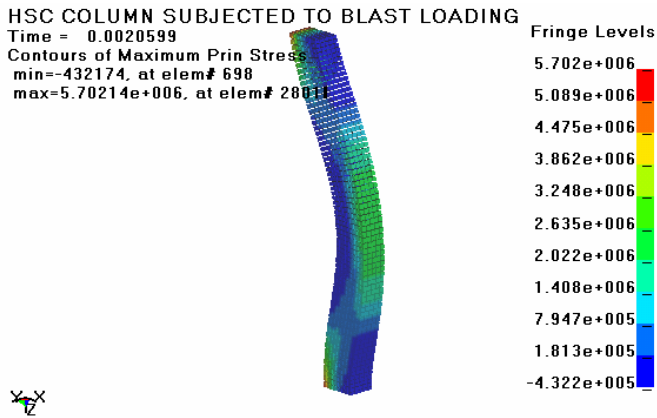
Figure 14. 3D model of the column using Explicit code LS-Dyna

The lateral deflection at mid point versus time history of two columns made of NSC and HSC are shown in Figs. 15 and 16. The graphs clearly show the lateral resistance of the columns. It can be seen that under this close-range bomb blast both columns failed in shear. However, the 80MPa columns with reduced cross section have a higher lateral deflection, which shows a better energy absorption capacity compared to that of the 40 MPa columns (see Fig. 17 and Table 4).

It can be seen from Figs. 15 and 16 that the effect of shear reinforcement is also significant. The ultimate lateral displacements at failure increase from 45mm (400 mm ligature spacing) to 63mm (100mm ligature spacing) for the HSC column. Those values for the NSC column are 20mm and 32mm, respectively.
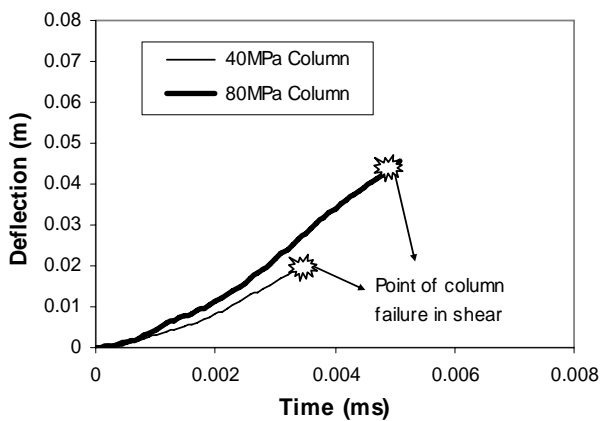
Figure 15. Lateral Deflection -Time history at mid point of column with 400mm ligature spacing (OMRF).
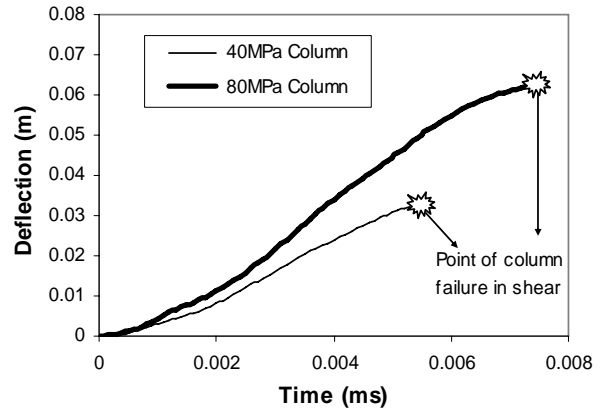
Figure 16. Lateral Deflection -Time history at mid point of column with 100mm ligature spacing (SMRF).
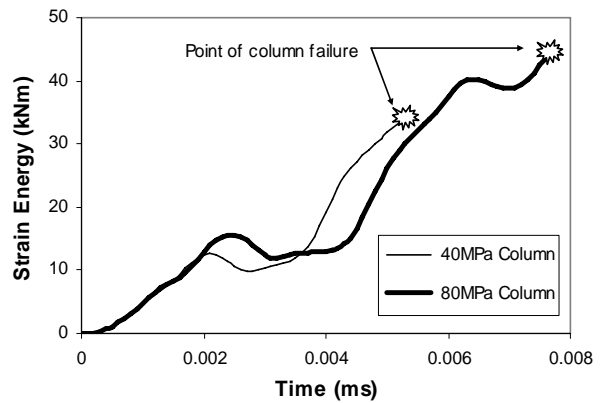
Figure 17. Comparison of energy absorption capacities (100mm ligature spacing).

Table 4. Energy absorptions at failure of HSC and NSC columns

Column	400mm spacing	100mm spacing
NSC	12.0 kNm	33.9 kNm
HSC	27.6 kNm	43.5 kNm

10.1 *Effect of strain-rate on ductility*

It is evident that increasing the rate of loading will result in increases in strength and stiffness of concrete, yield strength of steel and load-carrying capacity of reinforced concrete flexural members. A parametric study has been carried out to investigate the effects of high strain-rate on the ductility of reinforced concrete members, and on their flexural and shear capacities. The proposed strain-rate dependent model for concrete is adopted in this study. As shown in Fig. 18 the flexural capacity and the ductility of a reinforced concrete column were significantly increased due to the increase in yield strength of steel and compressive strength of concrete at high strain rate. The shear capacity of the column was calculated using the Modified Compression Field theory (Vecchio and Collins, 1986).
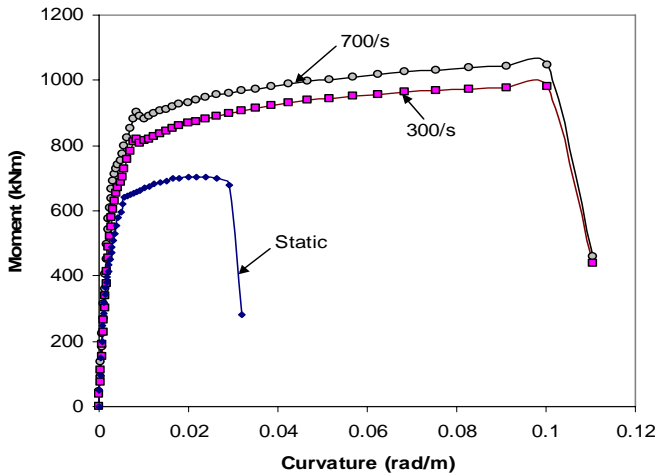
Figure 18. *M-φ* curves of a cross-section of a column at different strain rates

Fig. 19 shows the increased ratio of flexural capacity ($M_{u.dyn}/M_{u.stat}$) and shear capacity ($V_{u.dyn}/V_{u.stat}$) at high strain rate compared to those capacities under static loading. It can be observed from Fig. 19 that the increase in flexural strength was greater than that of shear strength. Thus, the increase in the material strengths under dynamic conditions may lead to a shift from a ductile flexural failure to a brittle shear failure mode.
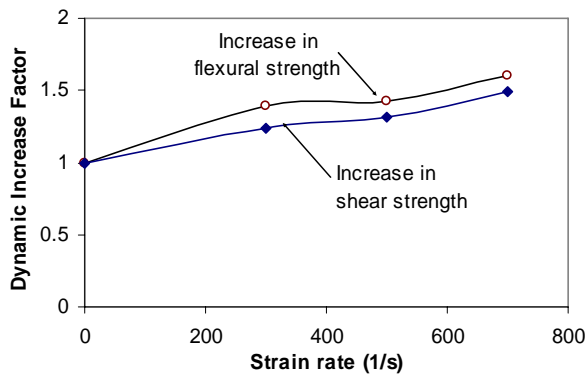
Figure 19. DIFs for flexural strength and shear strength of a column at different strain rates

11 CASE STUDY - PROGRESSIVE COLLAPSE ANALYSIS

Design recommendations on progressive collapse analysis have been introduced in British Standards since 1968, after the collapse of 22-storey Ronan Point apartment building. In recognition of this issue, a number of European countries, USA and Canada have incorporated progressive collapse provisions in their building codes. The American National Standards Institute (ANSI) Standard A58.1-1982, "Minimum Design Loads for Buildings and other Structures" recommends the alternative path method, in which the local failure is allowed to occur but an alternative path must be provided around the failed structural elements.

A 52 storey building (modified from a typical tall building designed in Australia) was analyzed in this study. The plan view and structural configuration of

the building are shown in Fig. 20. The typical story height is 3.85m. Perimeter columns are spaced at typical 8.4m centers and are connected by spandrel beams to support the facade. The lateral loads are resisted by 6 core boxes located at the centre of the structural plan. The building is designed to resist lateral loads due to wind and seismic ground motion specified by Australian Loading Standards AS1170.2 and AS1170.4. The slab, columns and core walls are all cast-in-place concrete. The lateral load resistance system (LLRS) of the building relies mainly on the lateral load capacity of the core walls which account for about 80% of the overall capacity.
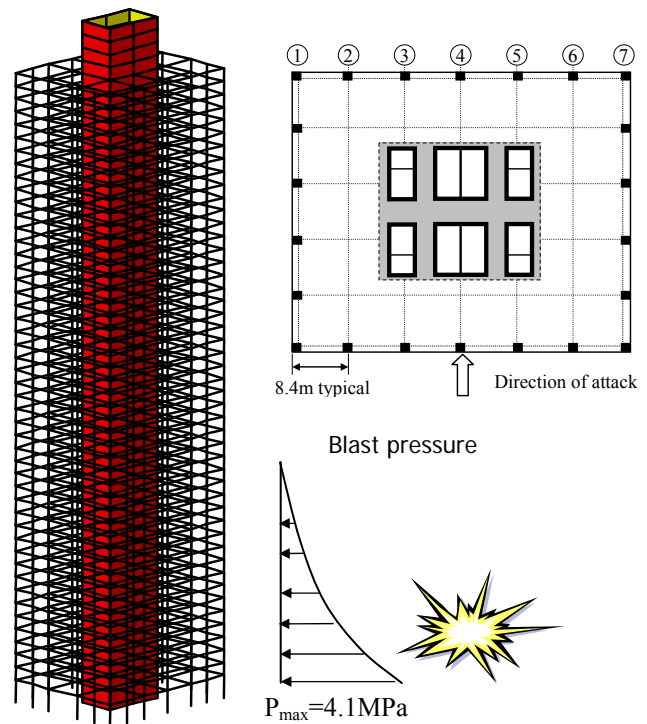
Fig. 20 Structural configuration

In this study which is based on the local damage assessment due to bomb blast at ground level, progressive collapse analyses was performed on the example building. The structural stability and integrity of the building were assessed by considering the effects of the failure of some perimeter columns, spandrel beams and floor slabs due to blast overpressure or aircraft impact. The main purpose of the analysis is to check if failure of any primary structural member will cause progressive collapse propagating beyond one story level above or below the affected member vertically, or to the next vertical structural member.
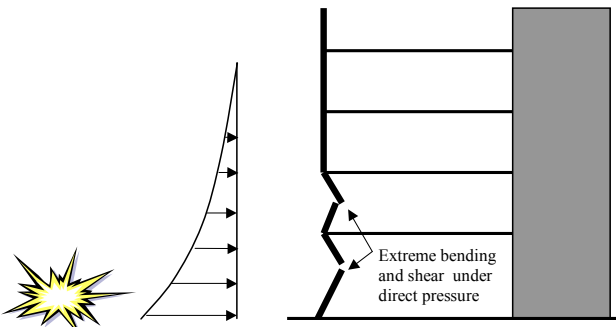
Fig. 21 Direct column loading (Blast pressure)
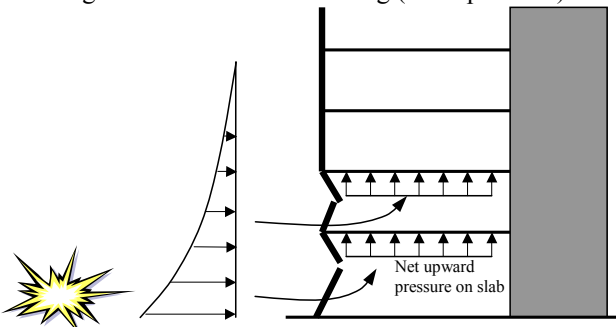
Fig. 22 Uplifting of floor slabs (Blast pressure)
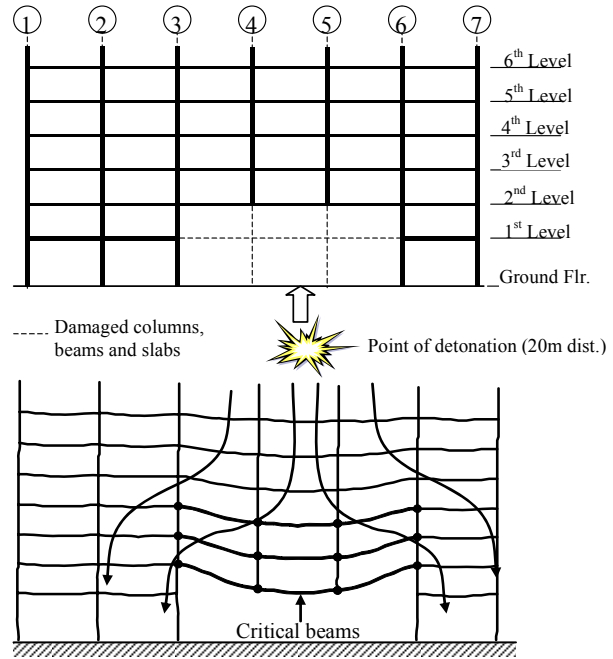
Fig. 23 Progressive collapse analysis of perimeter frame (damaged by blast load)

Figs. 21 & 22 show the effect of direct blast pressure on perimeter columns, beams and floor slabs. The concrete slabs in this example building are 125mm thick supported by prestressed wide band beams. The portion of floor slabs in close proximity to the blast were directly hit by the blast overpressure. The normal glazing façade offers insignificant resistance to the blast wave so after the failure of glazing, the blast fills the structural bay above and below each floor slab. The pressure below the slab is greater than the pressure above and causes the net upward load on each slab (Fig. 22).

To detect local damage, the blast analysis was carried out for perimeter columns, beams and floor slabs based on the actual blast pressures on each element. Results plotted in Fig. 23 show column lines 4, 5 of the ground and 1st levels failed due to the direct impact of the blast wave. Slabs and beams from column line 3 to 6 also collapsed. Member assessment was carried out using program RESPONSE (2001) based on the Modified Compression Field theory and LSDYNA (see section 10). More details are given elsewhere (Mendis & Ngo, 2002). The calculation also showed that if the columns were detailed using requirements for special moment resisting frames (SMRS) as given in ACI-318 Section 21, the shear capacity and the ductility would be improved significantly, thus improving the blast and impact resistance of the member. The damaged model of perimeter frame, in which failed elements were removed (Fig. 23), was analyzed to check if progressive collapse would propagate beyond one story level above or below.

As seen from Figs. 23, the alternative load paths go through columns surrounding the damaged area where the vertical loads are transferred. Beams and floor slabs above that area become critical due to the loss of the supporting columns. The overall stability of the structure will rely on continuity and ductility of these elements to redistribute forces within the structure. The falling debris of the collapsed members also imposes severe loading on the floors below. It is essential to check whether that overload can be carried without causing further collapse.

Parametric studies were also undertaken to investigate the impact resistance of the floor slab, assuming a floor above had collapsed onto it. The collapsing floor was treated as falling debris, i.e. the energy applied to the floor below was the weight of the collapsing floor multiplied by the height through which it fell. To obtain an estimate of the impact load-bearing capacity of the floor slab, the structure was analyzed using program LSDYNA. In addition to material and geometric nonlinearities, the analyses considered membrane action, inertia effects, and other influencing factors. The results show that the ultimate capacity of the floor slab is approximately 16.5kPa which is 2.75 times the total floor load (dead load plus 0.4 live load). Therefore in this case study if more than two floor collapsed, the falling debris of the collapsed members may impose an overload for the floor below and trigger a progressive collapse of the example building.

12 BLAST EFFECTS ON BUILDING'S FAÇADE

When a terrorist bomb explodes in an urban area, air blast pressure typically fractures lightweight façades

such as windows, causing catastrophic results. As a consequence of façade failure, the blast enters buildings, causing relatively superficial structural damage, but great disruption to the working environment and the mechanical and electrical services. Falling window glass shards cause injuries in addition to those resulting from blast pressure. Office fixtures and fittings are destroyed, and suspended ceiling and partitions are disturbed. Broken glass is projected everywhere, with particularly severe consequences for air conditioning systems.

Past events have shown that even relatively small explosions can cause significant window glass breakage, requiring as a minimum, window glass replacement and significant cleanup. Ideally, properly designed blast-resistant glazing should minimise, if not eliminate, flying and falling glass shards in any explosion. In addition, under air blast pressure loading, properly designed blast-resistant glazing should maintain closure of its fenestration, reducing cleanup costs and reducing pressure-related injuries. Even with blast-resistant glazing, air blast pressure will fracture windows, necessitating replacement. However, blast-resistant glazing should remain in its openings and reduce the urgency for immediate replacement.

Advanced computer codes such as CFD have been used to simulate the blast effects in the urban environment (Figs. 23, 24). A typical tall building subjected to a bomb blast detonated at different stand-off distances from the ground level was analysed in this study. The peak overpressure is 4.1MPa at the ground level and reduces rapidly up the height of the building. The average duration of loading was adopted as 15 milliseconds. Façade damage at different levels was assessed based on the blast pressure distribution and also using other in-house programs.
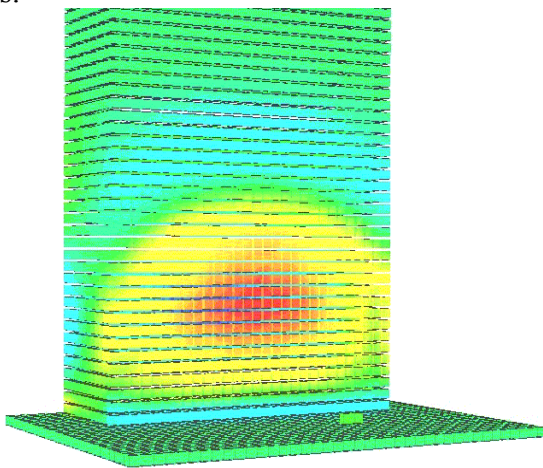
Fig. 24 CFD modelling of blast pressure on building structures (Mendis & Ngo, 2002)

Point of detonation (20m dist.)
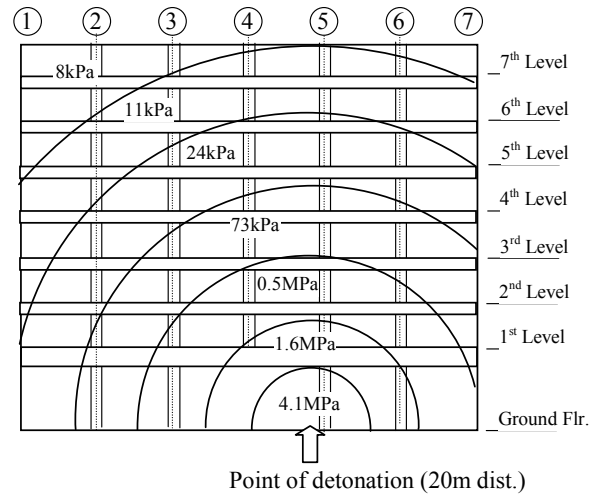
Fig. 25 Distribution of blast pressure on building façade (Mendis & Ngo, 2002)

There are only few guidelines developed to design blast-resistant façades. One of those is TM 5-1300, Structures to Resist the Effects of Accidental Explosions. In Section 6 of TM 5-1300, guidance is provided for the design, evaluation, and certification of windows to safely survive a prescribed blast environment described by a triangular-shaped pressure-time curve (Fig. 25). Window designs using monolithic (un-laminated) thermally tempered glass based on these guidelines can be expected to provide a probability of failure equivalent to that provided by current safety standards for safely resisting wind loads.

An example of a glazing system is illustrated in Fig. 25. The glazing is a rectangular, fully thermally tempered glazing panel having a long dimension, a; a short dimension, b; and thickness, t. The glass pane is simply supported along all four edges, with no in-plane and rotational restraints at the edges. The bending stiffness of the supporting elements of the panel is assumed to be an order of magnitude higher than that of the glass pane. Recent static and blast load tests indicate for a case in which the supporting frame deflects by up to 1/264 of the span distance, the glass pane resistance will not be significantly different to the ideal conditions of infinitely rigid supports.

The blast pressure loading is described by a peak triangular-shaped pressure-time curve as shown in Fig. 25. The blast pressure rises instantaneously to a peak blast pressure, B, and then decays linearly with a blast pressure duration, T. The pressure is uniformly distributed over the surface of the pane and applied normal to the pane.

The resistance function, r(X) (static uniform load, r as a function of centre deflection, X) for the plate accounts for both bending and membrane stresses. The effects of membrane stresses produce a nonlinear stiffness of the resistance-deflection function (Fig. 25). The design deflection, Xu is defined as the

centre deflection where the maximum principle tensile stress at any point in the glass first reaches the design stress, fun. Typically, as the deflection of the plate exceeds a third of its thickness, the points of maximum stress will migrate from the centre and towards the corners of the plate.

The model, illustrated in Fig. 25 uses a single-degree-of-freedom system to simulate the dynamic response of the plate. The model calculates the peak blast pressures required to exceed the prescribed probability of failure. The model assumes that failure occurs when the maximum deflection exceeds ten times the glazing thickness. More details of dynamic analysis of the glazing system can be found in TM5-1300.
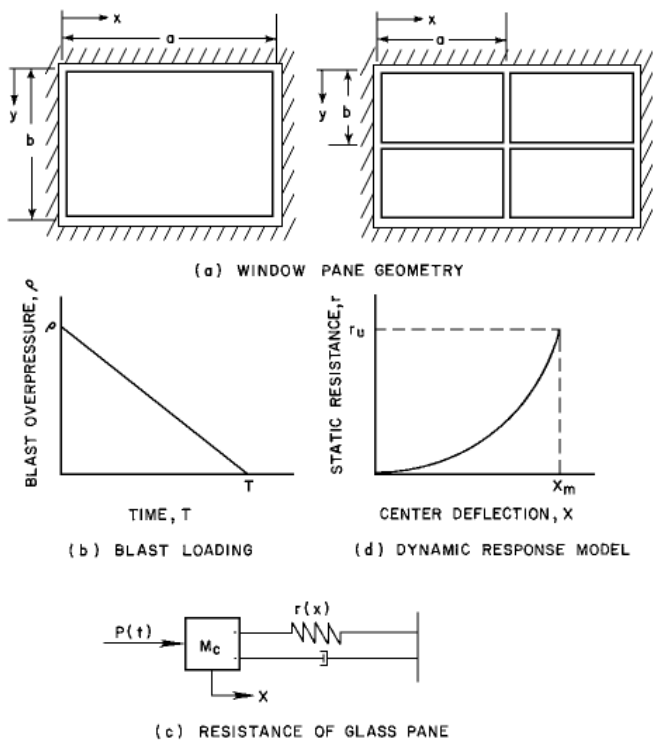
Figure 26 – Blast analysis for a glazing system

Design Charts

In TM5-1300, guidelines are also provided in the form of load criteria for the design of both the glass panes and framing system for the window. The criteria account for both the bending and membrane stresses and their effect on maximum principle stresses and the nonlinear behaviour of glass panes. The criteria cover a broad range of design parameters for rectangular-shaped glass panes. Design charts (see Fig. 26 as an example) are presented for monolithic thermally tempered glazing with blast overpressure capacity up to 690 KPa, an aspect ratio of $1.00 \leq a/b \leq 4.00$, pane area $0.1 \leq ab \leq 2.3$ m^2, and nominal glass thickness 6mm $\leq t \leq$ 20mm. An alternative method for blast capacity evaluation by

calculation is also provided in TM5-1300. This can be used to evaluate the blast capacity of glass when interpolation between charts is unadvisable, when design parameters are outside the limits of the chart.
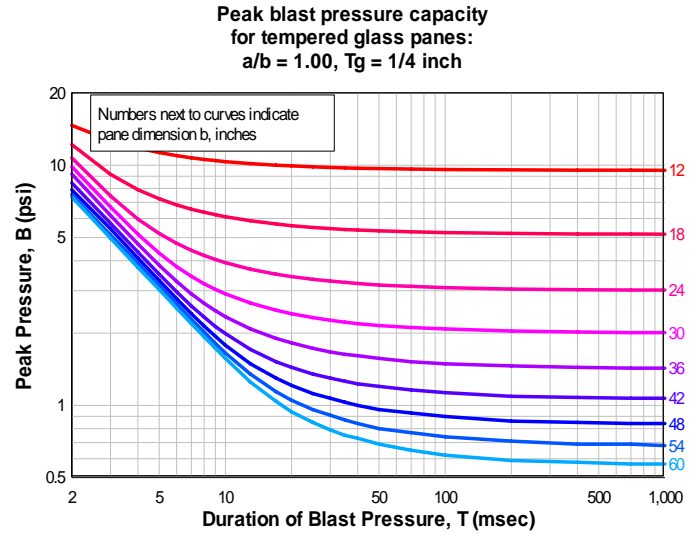
Figure 27 - A design chart for tempered glass panel (TM5-1300)

13 CONCLUSIONS

For high-risks facilities such as public and commercial tall buildings, design considerations against extreme events (bomb blast, high velocity impact) is very important. It is recommended that guidelines on abnormal load cases and provisions on progressive collapse prevention should be included in the current Building Regulations and Design Standards. Requirements on ductility levels also help improve the building performance under severe load conditions.

14 REFERENCES

1. Baker, W.E., Cox, P.A., Westine, P.S., Kulesz, J.J. and Strehlow, R.A., *Explosion hazards and evaluation,* Elsevier Scientific Publishing Company, New York, 1983.
2. Biggs, J.M, *Introduction to Structural Dynamics,* McGraw-Hill, New York, 1964.
3. Brode, H.L., "Numerical solution of spherical blast waves", *Journal of Applied Physics*, American Institute of Physics, Ney York, 1955.
4. Comité Euro-International du Béton, *CEB-FIP Model Code 1990*, Redwood Books, Trowbridge, Wiltshire, UK, 1990.
5. DAHS CWE, *Technical Manual - Design and Analysis of Hardened Structures to Conventional Weapons Effects,* U.S. Army Corps of Engineers (CEMP-ET), Washington DC, September, 1998.
6. DOE/TIC-11268. *A Manual for the Prediction of Blast and Fragment Loadings on Structures*, U.S. Department of Energy, Washington DC, 1992.
7. Dowling, A.R. and Harding, J., "Tensile properties of mild steel under high strain rates", *Proceedings of the 1st HERF Conf.*, University of Denver, Colorado, 1967.

8. Ellis, B.R. and Crowhurst, D., "The response of several LPS maisonettes to small gas explosions". *IStructE/BRE Seminar: Structural design for Hazardous Loads: The Role of Physical Tests*, Construction Press, New York, 1991.

9. ESL-TR-87-57, *Protective Construction Design Manual*, U.S. Air Force Engineering and Services Center, Tyndall Air Force Base, Florida, 1989.

10. Grote, D., Park, S., and Zhou, M., "Dynamic behaviour of concrete at high strain rates and pressures", *Journal of Impact Engineering*, Vol. 25, Pergamon Press, New York, pp. 869-886, 2001.

11. Longinow A, and Mniszewski KR., "Protecting buildings against vehicle bomb attacks", *Practice Periodical on Structural Design and Construction* , ASCE, New York, pp. 51-54, 1996.

12. LS-DYNA Version 960. 2002. Livermore Software Technology Corporation.

13. Malvar LJ., "Review of Static and Dynamic Properties of Steel Reinforcing Bars", *ACI Materials Journal*, 95(5), ACI, Detroit, Michigan, pp. 609-616, 1998.

14. Mendis, P.A., and Ngo, T. "Assessment of tall buildings under blast loading and aircraft impact", *Toward a better Built Environment, Innovation, Sustainability and Information Technology,* International Association of Bridge and Structural Engineering, Australia, pp. 375-376, 2002.

15. Mills, C.A., " The design of concrete structure to resist explosions and weapon effects," *Proceedings of the 1st Int. Conference on concrete for hazard protections*, Edinburgh, UK, pp. 61-73, 1987.

16. Milne-Thompson, L.M., *Theoretical Hydrodynamics*, McMillan, New York, 1968.

17. Newmark, N.M. and Hansen, R.J., "Design of blast resistant structures," *Shock and Vibration Handbook*, Vol. 3, Eds. Harris and Crede. McGraw-Hill, New York, USA. 1961.

18. Ngo, T., Mendis, P., & Itoh, A., "Modelling reinforced concrete structures subjected to impulsive loading using the Modified Continuum Lattice Model", *Proc. of 18th Australasian Conference on the Mechanics of Structures and Materials*, Perth, Australia. 2004b.

19. Ngo, T., Mendis, P., Hongwei, M. & Mak, S., "High strain rate behaviour of concrete cylinders subjected to uniaxial compressive impact loading", *Proc. of 18th Australasian Conference on the Mechanics of Structures and Materials*, Perth, Australia. 2004a.

20. Norris, G.H., Hansen, R.J., Holly, M.J., Biggs, J.M., Namyet, S. and Minami, J.K., *Structural design for dynamic loads*, McGraw-Hill, New York, USA. 1959.

21. TM 5-1300, *The Design of Structures to Resist the Effects of Accidental Explosions,* Technical Manual, US Department of the Army, Navy, and Air Force, Washington DC, 1990.

22. TM 5-855-1, *Fundamentals of Protective Design for Conventional Weapons*, U.S. Department of the Army, Washington DC, 1986.

23. Vecchio, F.J., & Collins, M.P. 1986. The Modified Compression Field Theory for Reinforced Concrete Elements Subjected to Shear, ACI Structural Journal, V83, 2, pp. 219-231.